Coordination Chemistry Reviews 253 (2009) 2328–2341

Contents lists available at ScienceDirect

Coordination Chemistry Reviews

journal homepage: www.elsevier.com/locate/ccr

Review

Strategies towards single molecule magnets based on lanthanide ions

Roberta Sessoli [a,*], Annie K. Powell [b]

[a] Department of Chemistry & INSTM, UdR Firenze, Univesità degli Studi di Firenze, Via della Lastruccia 3, 50019 Sesto Fiorentino, Italy
[b] Institut für Anorganische Chemie, Universität Karlsruhe, Engesserstrasse 15, D76131 Karlsruhe, Germany

Contents

ARTICLE INFO

Article history:
Received 1 October 2008
Accepted 16 December 2008
Available online 25 December 2008

Keywords:
Molecular magnetism
Lanthanides
Single molecule magnets
Clusters
Magnetic anisotropy

ABSTRACT

We review here the synthetic strategies employed in a concerted effort to obtain new single molecule magnets based on lanthanide ions in the framework of the research program on Molecular Magnetism funded by the Deutsche Forschungsgemeinschaft. The reported systems are grouped in 4f–2p, 4f–3d, and pure 4f materials. While the use of compartmentalized ligands, assisted self assembly, and site-targeted reactions have provided interesting examples of high nuclearity clusters, mostly characterized by large magnetic moments in the ground state, a deeper magnetic characterization of systems with smaller nuclearity has allowed us to gain evidence regarding the role played by weak exchange interactions and geometrical factors on the slow dynamics of the magnetization. In the case of a triangular cluster based on dysprosium the novel phenomenon of spin chirality has been observed.

1. Introduction

Lanthanides play a special role in magnetism, thanks to their large magnetic moments and in most cases huge magnetic anisotropy [1]. When present in what is usually their most stable trivalent oxidation state, there is the drawback of only a very weak exchange interaction as a result of the efficient shielding of the unpaired electrons in the 4f orbitals. This has resulted in only limited interest in the quest to create 3D molecular-based magnets using 4f ions exclusively and has led to the exploration of systems combining the 4f ions with other paramagnetic species such as organic radicals or 3d ions.

In complete contrast to this, for the case of slow-relaxing molecular units, which have been termed as single molecule magnets or SMMs [2], the fact that the magnetic anisotropy is a major component to see this effect has meant that the use of lanthanides has become of increasing interest. The interest in SMMs based on 4f ions was boosted by the report of Ishikawa et al. that slow relaxation of the magnetization is observable also in the case of mononuclear complexes [3], like the double-decker compound based on phthalocyanine, schematized in Fig. 1.

In the case of mononuclear complexes the difference between single molecule magnet behavior and normal paramagnetic relaxation is rather subtle. In fact slow relaxation of lanthanide ions had been widely investigated through *ac* susceptibility since the early days of cryogenic investigations at Kammerlingh Omnes laboratory in Leiden [4–6]. The application of a static magnetic field was necessary to monitor spin-lattice relaxation because in zero magnetic field transitions between opposite spin projections do not require

* Corresponding author. Tel.: +39 0554573268; fax: +39 0554573372.
E-mail address: roberta.sessoli@unifi.it (R. Sessoli).

0010-8545/$ – see front matter © 2009 Elsevier B.V. All rights reserved.
doi:10.1016/j.ccr.2008.12.014

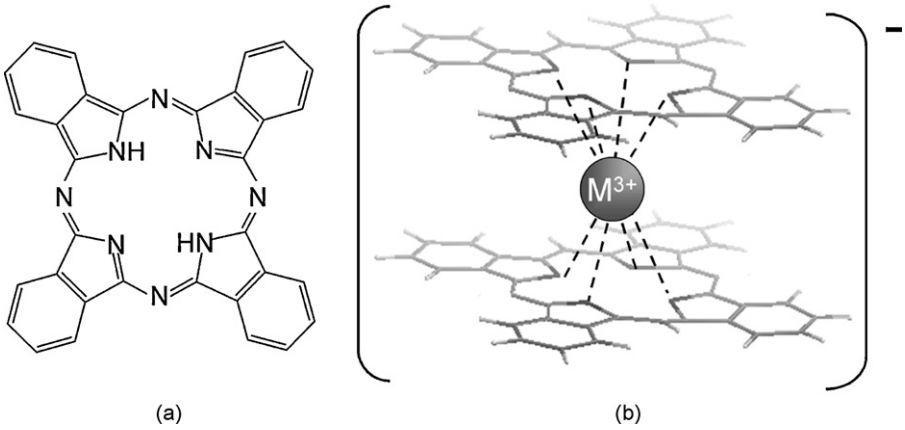

Fig. 1. (a) View of the structure of the phthalocyanine molecule. (b) Schematic structure of the double-decker $[(Pc)_2M]^-$ anion, where M is a lanthanide.

any energy exchange with the lattice and are therefore fast even at low temperature. The difference between a SMM and a normal paramagnet is in the probability of this direct transition being able to cancel any remnant magnetization, which is slow also in zero applied field because of the large S value. In the case of clusters comprising 3d metal ions the term that mainly affects the energy splitting of the spin multiplet, also known as zero field splitting, is given by

$$H = DS_z^2 \tag{1}$$

while higher order terms are often orders of magnitude smaller. This gives rise to the well known double well energy potential and the reversal of the magnetization has a characteristic time that increases exponentially on decreasing the temperature, according to the Arrhenius law:

$$\tau = \tau_0 \exp\left(\frac{\Delta E}{k_B T}\right) \tag{2}$$

The energy barrier to be overcome is of the order of DS^2 and $D(S^2 - 1/4)$ for integer and half-integer spins, respectively. Under barrier processes are also important but not to the extent for the case of a simple paramagnet. In fact the states characterized by the largest projection, $m_S = \pm S$, are admixed only at the 2Sth level of perturbation by any local transverse field.

In the case of lanthanide double-decker compounds the situation is more complicated. In fact, terms of different orders have comparable amplitude in the crystal field Hamiltonian [7]. Slow relaxation of the magnetization in zero static field has, however, been observed using *ac* susceptibility measurements at relatively high temperature [3,8,9]. This is probably a fortunate consequence of the tetragonal symmetry of the double-decker molecules, which reduces the admixing of sublevels characterized by opposite projection of the total angular momentum J, where $J = L + S$. On cooling, deviations from the Arrhenius law predicted for SMM behavior become, however, more and more important and hysteresis is only observed at very low temperature.

It is therefore interesting to pursue a rational approach to creating lanthanide-based SMMs to investigate what role the magnetic interaction between lanthanide ions can play in such a complicated scenario. Two different approaches have merged in a collaborative effort within the framework of the research project financed by DFG on "Molekularer Magnetismus". Small polynuclear complexes have been investigated in detail to elucidate the key role played by the magnetic interaction between lanthanide ions in addition to other geometrical factors. At the same time synthetic skills have been developed to increase the nuclearity of lanthanide-based clusters as well as to arrange them in extended structures and to explore new means of enhancing the SMM characteristics of 3d–4f systems. An overview of the main results achieved as an outcome of the complementarity of the two approaches and skills will be given in the following sections, without the aim of providing an exhaustive review of previous literature, covered by recent reviews [9–13].

2. Slow relaxation in 4f–2p systems

Among the several chemical approaches to molecular magnetic materials comprising rare earths a crucial role has been played by the combination of metal ions with paramagnetic ligands like nitronyl-nitroxide radicals [10,13,14]. Thanks to the strength of magnetic interaction promoted by these radicals, which have the unpaired spin density delocalized on the coordinating oxygen atoms, it has been possible to overcome the drawback in using weakly interacting trivalent lanthanides.

One of the most attractive features of nitronyl-nitroxide radicals is their capability to give one-dimensional structures where metal ions and bridging NITR radicals alternate [15]. The first systems investigated contain Gd^{III} and showed a behavior that could not be rationalized assuming either ferro- or antiferromagnetic metal–radical interaction. In fact in Gd–NITR systems the weak nearest neighbor ferromagnetic interaction is in competition with Gd^{III}–Gd^{III} and NITR–NITR next-nearest-neighbor antiferromagnetic interactions [16,17]. The spin structure of these strongly frustrated systems has a helicoidal arrangement with the pitch depending on the ratio between ferro- and antiferro-magnetic interactions. More recently a peculiar chiral 3d magnetic order has also been observed at low temperature [18,19].

Completely different is the case of strongly anisotropic metal ions such as Dy^{III}, Tb^{III}, and Ho^{III}. In this case one-dimensional compounds undergo transitions to magnetic order at relatively high temperatures, comparable to those observed in oxides and hydroxides [20–22]. When inter-chain exchange interactions are reduced these systems also exhibit slow relaxation of the magnetization in the paramagnetic phase, due to the short range correlation of the spins along the chain, thus enlarging what seems to be an ever-expanding range of magnetic phenomena observed in lanthanide-based molecular magnetic materials [23,24]. Systems exhibiting this novel behavior have been first observed in 3d–2p and pure 3d systems and have been termed single chain magnets [25–28].

Focusing our attention on SMMs, one of the simpler polynuclear complexes of lanthanides showing slow relaxation of the magnetization is based on the use of a nitronyl-nitroxide radical with an additional donor atom constituted by a pyridine nitrogen [29]. In the case of the compound of formula $[Ln^{III}(hfac)_3\{NITpPy\}]_2$

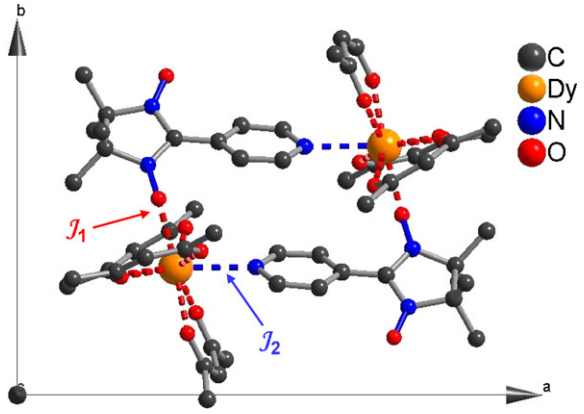

Fig. 2. Structure of the complex of formula $[M^{III}(hfac)_3\{NITpPy\}]_2$, where M = Gd^{III} or Dy^{III}, where the exchange interaction mediated by the oxygen atom and the pyridine nitrogen of the NIT-R radicals are labeled as J_1 and J_2, respectively. Crystallographic data available in Ref. [30].

(hfac = hexafluoroacetylacetonate and NITpPy = 2-(4-pyridyl)-4,4,5,5-tetramethyl-4,5-dihydro-1*H*-imidazolyl-3-oxide), the structure of which is depicted in Fig. 2 [30], each rare earth ion is coordinated to two radicals through two different donor atoms. This gives rise to a dimeric structure, referring to the metal nuclearity, while from the magnetic point of view it can be seen as a dimer of dimers. In fact for M = Gd^{III} the metal–radical exchange interaction through the oxygen atom of the radical, labeled as J_1 in Fig. 1, is ferromagnetic and equal to +2.6 K, where the isotropic exchange Hamiltonian has the form $H_{ex} = -JS_1S_2$. The exchange interaction occurring through the nitrogen of the pyridine ring is one order of magnitude weaker, being J_2/k_B = +0.24 K [30].

The substitution of the isotropic Gd^{III} ion with the anisotropic Dy^{III} leads to a more complex magnetic behavior, with an initial decrease on lowering the temperature from 300 K of the $\chi_M T$ product from the value expected for two ions with $^6H_{15/2}$ electronic state and two uncoupled $S = 1/2$ radicals. This is often seen for Dy^{III} and is due to the selective population of the lowest Kramers doublet of the $J = 15/2$ multiplet. At very low temperature it is rather common to treat the complex behavior of Dy^{III} as given by an effective $S_{eff} = 1/2$ with anisotropic exchange and an anisotropic **g** tensor to mimic the presence of a Kramers doublet well separated from the excited states. In most investigated Dy^{III} complexes the anisotropy is of the Ising type, i.e. $g_z \gg g_x, g_y$ and $J_z > J_x, J_y$, and the use of such an approximated Ising Hamiltonian, where only the z components are taken into account, has led to metal–radical ferromagnetic interactions of J_1/k_B = +18.7 K and J_2/k_B = +0.40 K. Despite the large differences in J_1 between the Gd and Dy isostructural derivatives, the exchange energy, proportional to JS_1S_2, is similar because of the difference in the spin values.

The derivative $[Dy(hfac)_3\{NITpPy\}]_2$ has been investigated as a possible SMM, and indeed frequency dependent *ac* susceptibility has revealed an out of phase component, χ'', even in zero static field [29]. In Fig. 2 the two components of the *ac* susceptibility as a function of temperature are shown. A strong frequency dependence is observed, but χ' and χ'' curves tend to level-off at low temperature. This is a typical indication that the dynamics become temperature independent. In this case the relaxation time can only be extracted by analyzing the frequency dependence of χ_{ac} at constant temperature, rather than from the more commonly employed χ'' vs. T curves. The extracted relaxation times, τ, are shown in Fig. 3 and reveal that below T = 1.7 K the relaxation time becomes temperature independent with a very gradual cross-over from a thermally activated, TA, regime to a quantum tunneling, QT, regime. The onset of the QT regime here occurs at much higher temperatures compared to that observed for clusters based on 3d ions, where low temperature investigations performed with a micrometric SQUID set-up often reveal temperature independent hysteresis curves only below 0.5 K [31].

The hypothesis that the observed change in relaxation regime is due to an underbarrier process involving direct transition between almost degenerate levels is confirmed by the marked increase in the relaxation time if a static magnetic field is applied. As shown in Fig. 3 the leveling of τ is suppressed and the entire curve is shifted to larger τ values. It is well-accepted that the application of an external field can remove the degeneracy of levels with opposite polarization of the magnetization and can suppress or reduce the tunneling efficiency, meaning that the system must overcome a larger barrier [2]. The additional marked shift in the pre-exponential factor, a feature often observed in SMMs, is not yet adequately investigated.

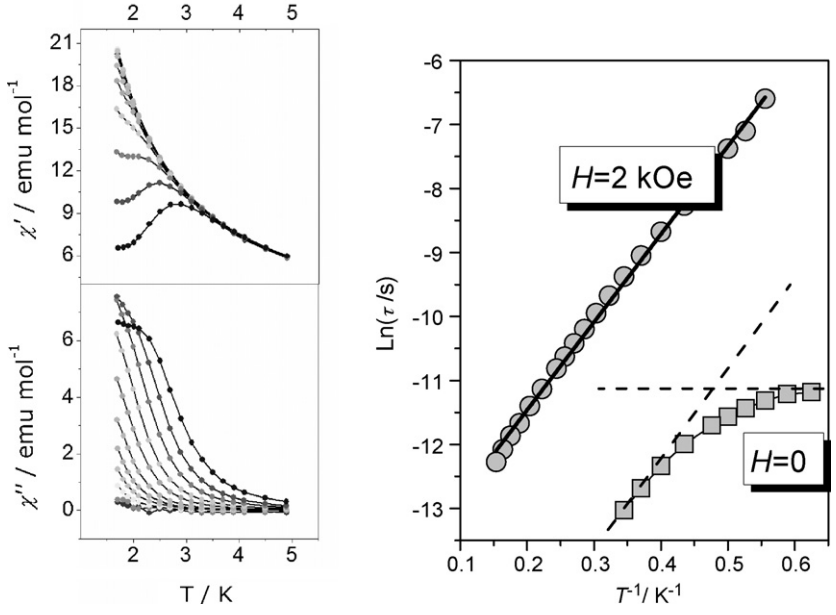

Fig. 3. The real and imaginary component of the *ac* susceptibility in zero static field of $[Dy^{III}(hfac)_3\{NITpPy\}]_2$ (left). The extracted relaxation times are drawn in the Arrhenius plot on the right, where the suppression of the tunneling due to the application of a static magnetic field is clearly evident. Redrawn from data of Ref. [29].

It is interesting to focus our attention on the role played by the weak interactions present in this dinuclear complex, in particular because, contrary to what is found for SMMs based on 3d metal ions, the magnetic anisotropy of the lanthanide ion is much stronger than any exchange interaction. Interestingly, the investigation of monomeric complexes of formula $Dy(hfac)_3(NITR)_2$ has not revealed any out-of-phase component of the *ac* susceptibility in similar frequency and temperature ranges. The modified coordination environment from DyO_7N to DyO_8, however, does not allow a direct comparison between the dynamic properties of the two types of compounds, dinuclear and mononuclear, respectively, where again the nuclearity refers to the number of metal ions. An alternative route to show if the dynamic behavior mainly arises from the isolated lanthanide ion or is significantly affected by the weak intra-cluster interactions is provided by the use of an admixture of diamagnetic $Y(hfac)_3{\cdot}2H_2O$ with a small percentage of $Dy(hfac)_3{\cdot}2H_2O$ in the reagents. The two metal ions, given their similar ionic radius, often give rise to isostructural complexes. In the ideal case, where the distribution of the two metal ions is fully random, the percentage of the Y–Y, Y–Dy, and Dy–Dy types of dinuclear complexes can be estimated from statistical consideration and only depends on the composition of the starting admixture. This is often not the case because small differences in the metal–radical affinity or solubility lead to a composition that deviates from the expected stoichiometry. A progressive enrichment of the solution in one of the components gives rise to an inhomogenous distribution of the two species, as recently detected using spatially resolved particle induced X-ray emission (PIXE) [32]. In the case of Dy-doping of a Y compound, however, the percentage of Dy^{III} can be safely assessed by the room temperature value of the magnetic moment. In the case of $[Y_{1-x}Dy_x(hfac)_3\{NITpPy\}]_2$ *x* has been found 0.15 instead of the stoichiometric value of 0.1 used in mixing the reagents.

Using this assumption, only 2.25% of the sample is constituted by Dy–Dy complexes with 25.5% of Dy–Y. This mixed species should then dominate the magnetic behavior of the doped sample, but no comparable imaginary component of the *ac* susceptibility can be observed in zero field. This confirms that, despite the weakness of the exchange interactions, the dynamics of the dinuclear species is significantly slower than that of an isolated lanthanide ion in the same crystal field. This could be a taken as a foregone conclusion, but we will show in the next section that it is not indeed the case.

3. 4f–3d systems

Practically at the beginning of research into molecular-based magnetism it was predicted that mixing 3d and 4f ions could lead to systems showing the sort of interesting magnetic behavior observed for bulk magnets combining metal ions from these areas of the Periodic Table. However, early forays proved disappointing since, on one hand, the interactions were rather weak and, on the other, the synthesis of such mixed-metal compounds was more complicated than envisaged. In fact, until relatively recently, most mixed 3d–4f systems, especially for discrete molecular clusters, were restricted to Cu/Gd compounds [33,34]. Many attempts to combine 3d and 4f ions resulted in them forming their own all 3d or all 4f coordination compounds with little in the way of mixed systems observed. Furthermore, synthetic chemists did not immediately realize that the special nature of lanthanide ions means that a survey across all available 4f ions is a requirement of this research. This is the consequence of the very different nature of the influence that the ligand field plays for 3d and 4f metals. For the classic coordination chemist, 3d metal ions provide the archetypes which can be described using a ligand field description of electronic structure. For 4f metal ions, such a description is no longer really useful and understanding the electron distribution amongst the f orbitals in conjunction with significant spin–orbit coupling makes it difficult to give the clear answers provided by Ligand Field Theory for the 3d metal ions. We purposely do not consider 4 and 5d metals or 5f actinides here, because such research is still largely unexplored, with so far only a preliminary result of a $[Re^{V}{}_2Y_2]$ linear cluster reported in the framework of the DFG funded project [35]. Moreover, heavier transition metal ions have very different electronic structures from what we discuss here, which, in terms of trying to understand their magnetic interaction, will require yet further development beyond simple Russell-Saunders type coupling schemes.

Nevertheless, research in recent years has provided a good number of compounds containing both 3d and 4f ions showing slow relaxation of the magnetization [36–50]. In the case of isolated molecules it has been possible to begin to understand the roles played by the two different sorts of ions in producing magnetically interesting molecules.

3.1. Synthetic strategies

From a synthetic point of view, ways must be found to combine 3d and 4f ions within a coordination compound. Experience has shown that simply mixing the components does not lead to the self-assembly of the desired mixed compounds, but mostly to pure 3d compounds. This is probably the result of the ligand field stabilization for 3d compounds being a driving force. To circumvent this two fruitful approaches have been developed. One is to design ligands which provide coordination pockets capable of both coordinating and connecting the different types of metal ion centers. In the other an assisted self assembly approach is used where lanthanide ions combine with 3d transition metal ions deriving from polynuclear species in the presence of further coligands which can also provide suitably stabilizing counterions/ligands to drive the reaction. More recently, a "site-targeted" strategy has been proposed and developed. This allows mixed 3d–4f molecules to be investigated where either the 4f or 3d sites can be swapped for different respective ions in order to gauge the influence that both can have on the magnetic properties of the resulting system.

3.1.1. Compartmentalized ligands

In this approach compartmentalized ligands are synthesized with the aim of capturing and linking different types of paramagnetic centers to produce magnetically interesting systems. Thus, for example, a ligand can be designed to provide a coordination environment favored by a 3d metal such as Mn^{III} or Cu^{II} (relatively N rich) as well as a site (relatively O rich) more favored by a "hard" metal ion such as Fe^{III} or any Ln^{III}.

Schiff-base ligands are useful in this approach since they are easy to tailor. For example, combining *o*-vanillin and tris (hydroxymethyl) aminomethane to give the ligand (H_4L, Scheme 1) provides a system which captures two Gd^{III} and five Cu^{II} ions in $[Gd_2Cu_5(OH)_4(Br)_2(H_2L)_2(H_3L)_2(NO_3)_2(OH_2)_4]^{2+}$ (see Fig. 4) [51]. While this ligand had been previously used to prepare homometallic clusters [52], it seemed reasonable to hope that

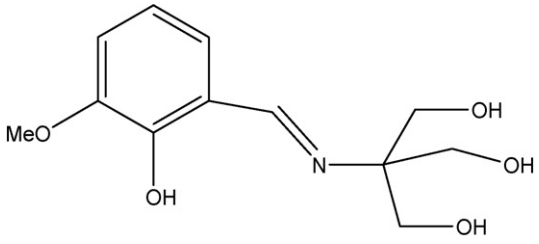

Scheme 1. A Schiff base ligand derived from *o*-vanillin.

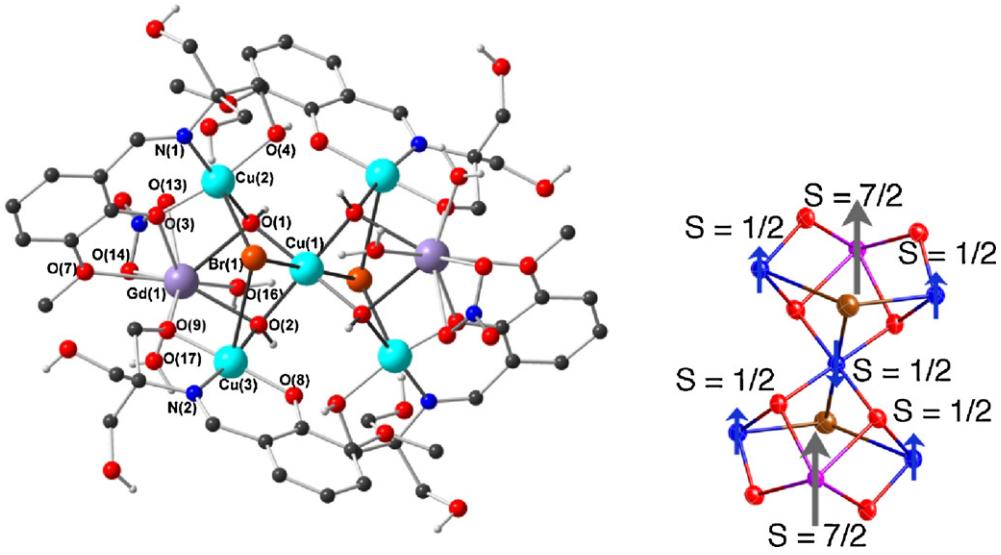

Fig. 4. (Right) Structure of the $[Gd_2Cu_5(OH)_4(Br)_2(H_2L)_2(H_3L)_2(NO_3)_2(OH_2)_4]^{2+}$. The C–H hydrogen atoms have been omitted for clarity. (Left) Spin topology of the core. Redrawn from Ref. [51].

the oxygen-donor-rich tripodal tris(hydroxymethyl) aminoethane derived group would capture the oxophilic lanthanide, whereas the Cu^{II} ions would be coordinated by both the imine nitrogen and oxygen donors. Magnetic studies on this system showed that ferromagnetic interactions dominate although the spin of the central Cu^{II} is antiparallel to all the other spins in the core leading to an overall isotropic $S = 17/2$ ground state.

So far this approach has led to some high spin molecules, mostly comprised of Gd^{III} plus 3d ions. In this respect, the Gd^{III} ion seems to act as an honorary 3d-transition metal ion and such compounds are apparently relatively accessible. This might be the result of the ion being rather isotropic and perhaps somewhat akin to isotropic 3d ions such as high spin Mn^{II} and Fe^{III} or else simply a result of the fact that the salts of Gd^{III} are easy to handle, relatively cheap and of defined stoichiometry; in other words, a reflection of the fact that the other 4f metals in the series still remain to be explored. As we will see later, recent work in this area indicates that Gd^{III} tends to mark a turning point when surveying the compounds formed in mixed 3d–4f systems, or, indeed, pure 4f systems. In general, the first half of the lanthanide series will form one set of isostructural compounds and the latter half is likely to crystallize in a different isomorph. Often, Gd^{III} will form structures belonging to both groups.

The choice of the ligand determines if the outcome of a synthesis can be easily predicted as in the case of the ligand corresponding to the anionic form of bis(2-pyridylcarbonyl)amine, $pbca^-$, shown as a scheme in Fig. 5 [53]. With its two pockets comprising different hard–soft acid character it can be used to obtain structures with heterometallic motifs, and gives rise to dimeric species [54], trimeric species [55,56], and extended structures [57–60]. The pbca-ligand has been used to bridge different 3d ions or to alternate them with lanthanides. The first reported SMM based on this ligand has formula $[Fe^{III}(bpca)(\mu\text{-}bpca)Dy(NO_3)_4]$ [54].

On the contrary, the reaction of the preformed $[M^{II}(bpca)_2]$ complex again with $Dy(hfac)_3{\cdot}2H_2O$ leads to the formation of a trimeric species of formula $[\{Dy(hfac)_3\}_2M^{II}(bpca)_2]$ [61], with the two water molecules on each lanthanide ion replaced by the β-diketonate arm of the bpca ligand, as shown in Fig. 5. The use of Fe^{II}, which has low spin configuration, and of Ni^{II}, with $S = 1$, allows to compare the magnetic behavior of two practically isolated Dy^{III} ions with those of a coupled species where weak but sizeable ferromagnetic interaction between Ni^{II} and Dy^{III} are present.

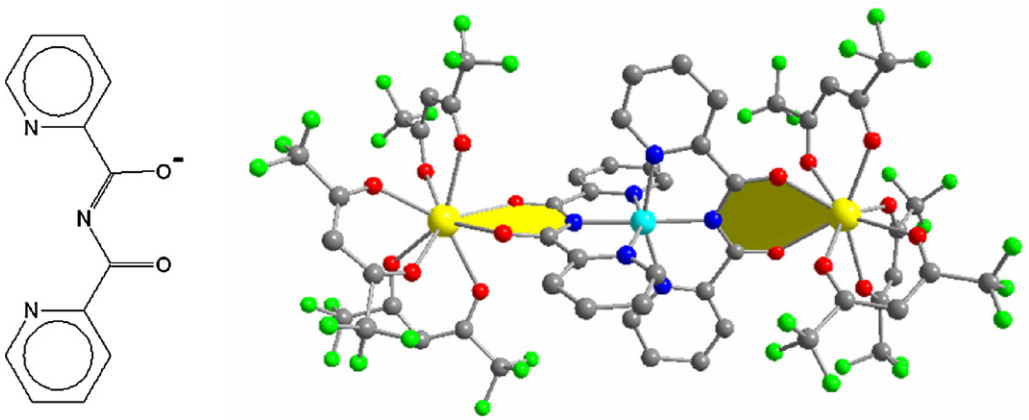

Fig. 5. (Left) Scheme of the bi-compartmental ligand bis(2-pyridylcarbonyl)amine anion, $pbca^-$. (Right) Structure of the trinuclear complex $[\{Dy(hfac)_3\}_2M^{II}(bpca)_2]$, where Dy atoms are in yellow, the bivalent 3d ion in cyano, C, N, O, F are in grey, blue, red, and green, respectively. The orthogonal arrangement of the Dy coordination polyhedra is depicted by the shading. Crystallographic data available in Ref. [61].

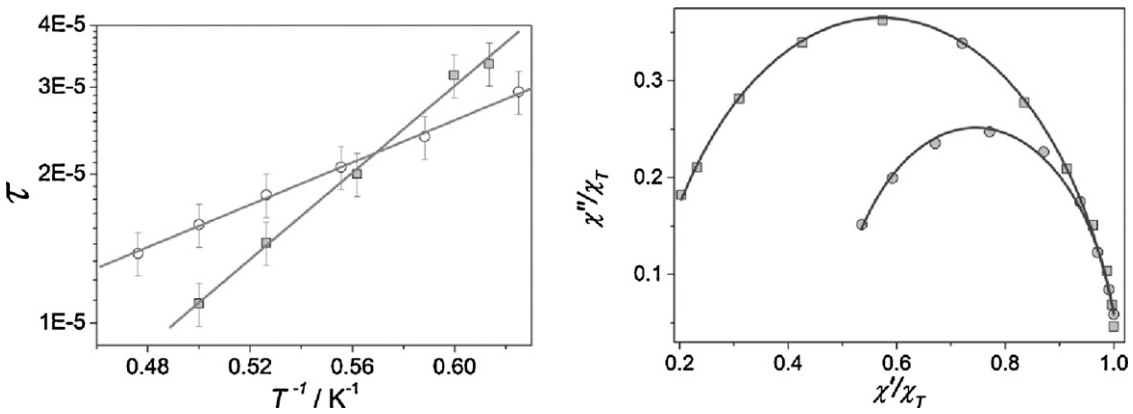

Fig. 6. (Left) Arrhenius plot extracted for the [Dy_2Fe] (squares) and [Dy_2Ni] (open circles) trinuclear complexes. Linear regression performed on the data gave $\Delta E/k_B = 9.7 \pm 0.4$ K and 4.9 ± 0.3 K for [Dy_2Fe] and [Dy_2Ni], respectively. (Right) Argand diagram taken for [Dy_2Fe] (squares) and for [Dy_2Ni] (open circles) at $T = 1.6$ K. The lines represent the best-fit calculated values with an extended Debye model providing: $\alpha = 0.12 \pm 0.03$ for [Dy_2Fe] and $\alpha = 0.03 \pm 0.01$ for [Dy_2Ni]. Redrawn from data of Ref. [61].

The *ac* susceptibility in zero static field shows a very weak out-of-phase signal for [Dy_2Fe] with a low ratio of χ''/χ' and an almost undetectable one for [Dy_2Ni], as indeed observed in Ref. [12] for the previously mentioned $Dy^{III}Fe^{III}$ binuclear complex. The application of a static field allows for the observation of well developed maxima in the χ'' vs. frequency curves and thus to extract the relaxation times shown on the left of Fig. 6. Even in the limited range which can be investigated, the differences between [Dy_2Ni] and [Dy_2Fe] are remarkable, with a barrier in the Arrhenius plot that is almost reduced to a half for the species where exchange interaction is active, in contrast with what was observed in the metal-radical complexes previously described.

A possible explanation of this counterintuitive effect, i.e. the coupled system relaxing faster than the uncorrelated spins system, can be found in the geometrical arrangement of the dysprosium coordination polyhedra that are mutually orthogonal as evidenced by the shading in Fig. 5. This is a direct consequence of the orthogonal coordination of the two $bpca^-$ ligand around the divalent metal ion. Unless the unique case, where the easy axis of Dy^{III} lies along the Dy-M direction, is accidentally encountered the anisotropy axes of the two coupled Dy ions are expected to be non-collinear, in contrast to what happens in the case of $[Dy(hfac)_3\{NITpPy\}]_2$ or in a [Dy_2Cu] trimer [62], where the two lanthanide coordination polyhedra are collinear being related by an inversion center.

The difference between the two complexes is even more striking in Fig. 6(right) where the imaginary component of the *ac* susceptibility, χ'', is shown graphically vs. χ' in the so-called Argand or Cole–Cole plot [63,64]. This type of plot is particularly useful to quantify the width of the distribution of the relaxation times. In fact the Debye theory predicts that if the whole magnetization relaxes with a single characteristic time the curve describes a semicircle whose center lies on the χ' axis. A flattening of the curve denotes the presence of a distribution of relaxation times and can be accounted by an empirical parameter, α in the expression of the complex susceptibility [63,64]:

$$\chi(\omega) = \chi_S + \frac{\chi_T - \chi_S}{1 + (i\omega\tau)^{1-\alpha}}$$

and

$$\chi'(\omega) = \chi_S + (\chi_T - \chi_S)\frac{1+(\omega\tau)^{1-\alpha}\sin(\alpha\pi/2)}{1+2(\omega\tau)^{1-\alpha}\sin(\alpha\pi/2)+(\omega\tau)^{2-2\alpha}},$$
$$\chi''(\omega) = (\chi_T - \chi_S)\frac{(\omega\tau)^{1-\alpha}\cos(\alpha\pi/2)}{1+2(\omega\tau)^{1-\alpha}\sin(\alpha\pi/2)+(\omega\tau)^{2-2\alpha}} \quad (3)$$

the isothermal, χ_T, and adiabatic, χ_S, susceptibilities that can be seen as the susceptibility observed in the two limiting cases for the *ac* frequency tending to zero and infinity, respectively.

These two parameters can be extracted as the two intercepts of the semicircle with the χ' axis, being obviously constrained such that $\chi_T > \chi_S$, by fitting the experimental curve with the following expression:

$$\chi'' = \frac{1}{2}(\chi_S - \chi_T)\tan\left(\frac{\pi}{2}\alpha\right) + \frac{1}{2}\sqrt{\left[(\chi_T - \chi_S)\tan\left(\frac{\pi}{2}\alpha\right)\right]^2 - 4\left[\chi'^2 - \chi'(\chi_T + \chi_S) + \frac{1}{4}(\chi_T + \chi_S)^2 - \frac{(\chi_T - \chi_S)^2}{4(\sin(\pi/2)(1-\alpha))^2} + \frac{1}{4}(\chi_T - \chi_S)^2\left(\tan\left(\frac{\pi}{2}\alpha\right)\right)^2\right]} \quad (4)$$

The analysis of the data on the right of Fig. 6 provides rather small values of the α parameters, 0.12 and 0.03 for [Dy_2Fe] and [Dy_2Ni], respectively, suggesting that the systems show a low degree of disorder. However, the two curves are very different in terms of the ratio χ_S/χ_T, which is almost zero for [Dy_2Fe] but 0.5 for [Dy_2Ni].

This observation suggests that in [Dy_2Ni] half of the susceptibility is able to relax freely even at the highest frequencies investigated, and that this occurs in the absence of disorder. It could be argued that the fast relaxing component of the magnetization is associated to the central nickel ion. However, its amplitude, corresponding to $\chi T \sim 4$ emu K mol^{-1}, largely exceeds the contribution expected for an $S = 1$ spin.

A possible explanation can be found, again, in the peculiar orthogonal arrangement of the Dy^{III} coordination polyhedra. In the case of [Dy_2Fe], where the Dy^{III} magnetic moments are uncorrelated, experiments on powder samples probe the random distribution of orientations of the easy-axes of magnetization with respect to the applied field. Only the component along the easy-axis is expected to experience an energy barrier for its reversal and thus give rise to slow relaxation. The transverse components are, on the contrary, expected to give rise to fast relaxation. In a Dy^{III}-based system these components will, however, be very small because g_x and g_y are much smaller than g_z. If two Dy^{III} ions are exchange-coupled through a paramagnetic 3d bridging ion, as in [Dy_2Ni], but have non-collinear easy axes, the resultant magnetic anisotropy can still be of the easy axis type. Now the transverse component of the

susceptibility can be significantly larger than that observed for an isolated Dy^{III} ion. As the hard components do not experience any barrier for their reversal their relaxation is fast and gives rise to a much larger χ_S/χ_T ratio, as indeed experimentally observed in [Dy_2Ni] [61].

Non-collinearity of the magnetic anisotropy tensors is a rather common feature in molecular magnetism as a consequence of the intrinsic low symmetry of the coordination sites compared to inorganic structures. It is responsible for transverse magnetic anisotropy in the archetypal SMM based on Mn_{12} clusters [65] and is the key ingredient in weak-ferromagnetism, recently exploited also in the other class of slow-relaxing molecular nanomagnets, i.e. single chain magnets [66]. We will see in the following sections that non-collinear magnetic structures, if combined with the huge anisotropy of some lanthanides, can provide novel magnetic phenomena, such as spin chirality.

3.1.2. Assisted self assembly reactions

Preformed 3d metal carboxylato aggregates can be combined with simple metal salts in the presence of N-substituted diethanolamine ligands, possibly with further coligands, to produce larger aggregates. This type of approach has been successfully applied by a number of groups to produce larger 3d clusters [67] and it was recently shown to be a useful method for combining 3d and 4f metals within one aggregate [68,69].

Thus the isostructural cluster anions of general formula $[Fe^{III}_5Ln_8(\mu_3\text{-}OH)_{12}(L)_4(piv)_{12}(NO_3)_4(OAc)_4]^-$ for Ln = Pr, Nd and Gd and where $piv^- = CMe_3CO_2^-$, were synthesized by reaction of ^{n}Bu-deaH$_2$ with $[Fe_3O(piv)_6(H_2O)_3](piv)$ and $Ln(NO_3)_3{\cdot}xH_2O$ in the presence of $NaOAc{\cdot}3H_2O$ [70].

With reference to the structure for the Gd^{III} containing compound, the $[Fe^{III}_5Ln^{III}_8]^{39+}$ core is held together by 12 μ_3-OH ions (Fig. 7). Peripheral ligation is provided by 4 chelating/bridging (μ_3:η^1:η^2:η^2) bdea^2, 12 bridging (μ:η^1:η^1) piv, 4 bridging (μ:η^2:η^1) $MeCO_2$ and 4 chelating and bridging (μ:η^1:η^1) NO_3 ligands. The core of the centrosymmetric tridecanuclear cluster can be viewed as consisting of two distorted inner heterometallic $[FeGd_3(\mu_3\text{-}OH)_4]^{8+}$ cubane units sharing a common vertex Fe(1), flanked by four edge-sharing heterometallic $[FeGd_2(OH)_4]^{5+}$ partial cubane units. Six of the eight Gd^{III} ions are arranged in a planar hexagonal ring capped above and below the plane by the other two Gd(1) and Gd(1′), all five Fe^{III} are close to coplanar with four Fe^{III} atoms located at the vertices of a rectangle and the fifth at the center. This central Fe^{III} ion, Fe(1), lies on a crystallographic inversion center. Two types of bridging pivalate (Gd/Gd and Gd/Fe) can be identified. Thus the trinuclear iron starting material provides pivalate coordination to the lanthanide ions. Furthermore, the acetates introduced from the sodium acetate link the ring Gd ions in a μ_2:η^2:η^1 fashion, and the nitrates chelate exclusively to the out of plane Gd ions. Overall, each of the four peripheral Fe^{III} ions is bridged to two Ln centers by two μ:η^1:η^1 pivalate ligands, one μ_3-OH ion, and two μ-oxygen atoms from a ^{n}Bu-dea^2 ligand, while the central Fe^{III} ion is bridged to six Ln ions through six μ_3-OH groups. All the Fe atoms are 6-coordinate, exhibiting a distorted octahedral coordination geometry through six μ_3-OH ligands for the central Fe(1) atom, and an NO_5 chromophore consisting of a O_2N donor set from a ^{n}Bu-dea^2 ligand moiety, one μ_3-OH group, and two bridging pivalate oxygen atoms, for the peripheral Fe atoms. In contrast, the Ln atoms show three different types of coordination geometries: *types* I and II, 9-coordinate, and *type* III, 8-coordinate, all varying in their coordination environment. This underlines that the assisted self assembly approach involves providing sufficient ligating and bridging species to satisfy the Ln coordination sphere. It can also be noted that the hydrolysis of water to provide the hydroxide bridges is an important feature of this chemistry.

The *dc* magnetic susceptibility measurements were carried out on polycrystalline powder samples in the 1.8–300 K temperature range. The plots of χT vs. T are shown in Fig. 8. At room temperature, the χT product is 31.8, 35.4, and 81.5 emu K mol^{-1} for $[Fe_5Pr_8]$, $[Fe_5Nd_8]$ and $[Fe_5Gd_8]$, respectively. On lowering the temperature, the χT product of the Pr^{III} and Nd^{III} complexes slowly decreases reaching 17.2 emu K mol^{-1} and 25.8 emu K mol^{-1} at 4.2 and 9 K, respectively. At lower temperature, the χT product at 1000 Oe increases to a maximum value at 1.8 K of 19.9 emu K mol^{-1} and 42 emu K mol^{-1}, respectively. For Gd_3, the temperature dependence of the χT product at 1000 Oe is qualitatively different. Indeed, the χT product continuously increases when the temperature is lowered down to 1.8 K to reach 130.2 emu K mol^{-1}. The fit of the experimental data to a Curie–Weiss law leads to the following Curie and Weiss constants: 32.4 emu K mol^{-1} and −6.5 K for $[Fe_5Pr_8]$ (above 15 K), 36.8 emu K mol^{-1} and −13.8 K for $[Fe_5Nd_8]$ (above 60 K), and 80.7 emu K mol^{-1} and +1.0 K for $[Fe_5Gd_8]$ (down to 2 K). The Curie constants are in relatively good agreement with the expected values: 34.675, 35.0, and 84.875 emu K mol^{-1} for $[Fe_5Pr_8]$, $[Fe_5Nd_8]$ and $[Fe_5Gd_8]$, respectively, considering five $S = 5/2$ Fe^{III} ($C = 4.375$ emu K mol^{-1} with $g = 2$) and eight Pr^{III} ($S = 1$,

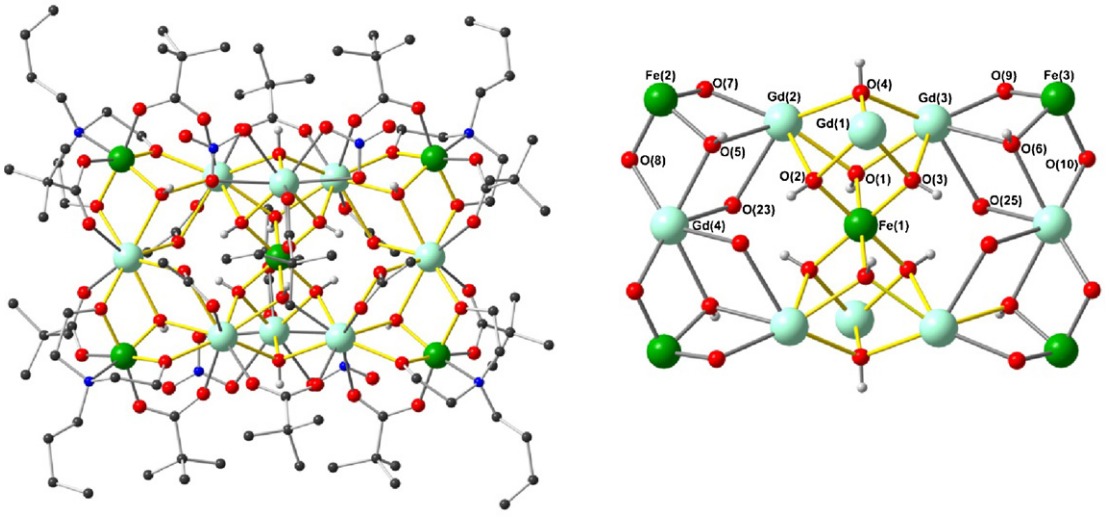

Fig. 7. Structure of the anion $[Fe^{III}_5Gd_8(\mu_3\text{-}OH)_{12}(L)_4(piv)_{12}(NO_3)_4(OAc)_4]^-$ (left) and the core (right). Hydrogen atoms apart from the core have been omitted for clarity. Color code: Fe (green), Gd (turquoise), N (blue), O (red), C (grey), and H (white). Structural data available in Ref. [70].

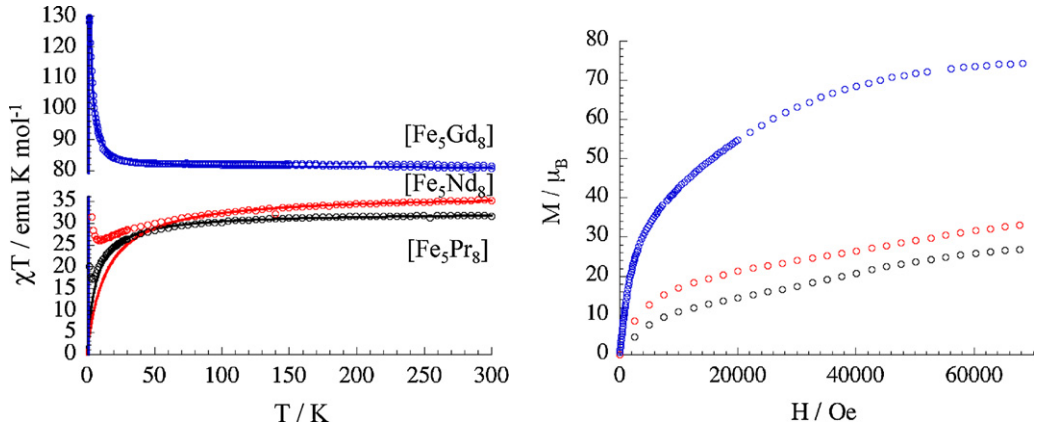

Fig. 8. Temperature dependence of the χT product at 1000 Oe (left) and the field dependence of the magnetization at 1.85 K (right) for $[Fe_5Pr_8]$, $[Fe_5Nd_8]$ and $[Fe_5Gd_8]$. Adapted from Ref. [70]. Solid lines correspond to the fits described in the text.

$L = 3$, $^3H_4$, $g = 4/5$: $C = 1.60$ emu K mol^{-1}) or eight Nd^{III} ($S = 3/2$, $L = 3$, $^4I_{9/2}$, $g = 8/11$: $C = 1.64$ emu K mol^{-1}) or eight Gd^{III} ($S = 7/2$, $C = 7.875$ emu K mol^{-1} expected for $g = 2$).

The negative Weiss constants obtained for $[Fe_5Pr_8]$ and $[Fe_5Nd_8]$ suggest the presence of dominant antiferro-magnetic interactions between spin carriers with a possible ferrimagnetic arrangement revealed by the low temperature increase of the χT product. It should be added that the effects of the thermal depopulation of Pr^{III} and Nd^{III} excited states that result from spin–orbit coupling and a low symmetry crystal field, might also be partially responsible for the decrease of the χT product when the temperature is lowered. In contrast for $[Fe_5Gd_8]$ the positive Weiss constant indicates the presence of dominant ferromagnetic interactions between Fe^{III} and Gd^{III} metal ions. These interactions are weak as indicated by the small value of the Weiss constant (1.0 K), but in principle they could stabilize a high spin ground state at very low temperature. The field dependence of the magnetization at 1.85 K was measured for this series of compounds. For $[Fe_5Pr_8]$ and $[Fe_5Nd_8]$ the lack of saturation on the M vs. H data, especially at 1.8 K, suggests the presence of magnetic anisotropy or more likely low lying excited states induced by weak intra-complex magnetic coupling between magnetic centers. For $[Fe_5Gd_8]$, the magnetization seems almost saturated at 70 kOe to 74.4 μ_B, which is lower than the value of 81 μ_B expected if all the spins are ferromagnetically aligned. Therefore, although ferromagnetic interactions are dominant in $[Fe_5Gd_8]$, the presence of antiferro-magnetic interactions leads to a large spin ground state slightly lower than the maximum possible of 81/2. It is also worth mentioning that the M vs. H data even at 1.8 K do not show any sign of magnetization slow relaxation, i.e. hysteresis effects. In concordance with this, the *ac* susceptibility of these compounds in zero *dc* field shows a complete absence of out-of-phase components above 1.8 K.

Using a similar strategy, the preformed hexanuclear Mn complex, $[Mn^{III}_2Mn^{II}_4O_2(piv)_{10}(4\text{-Me-py})_{2.5}(pivH)_{1.5}]$ was used as a source of $Mn^{II/III}$ ions. Reaction of this with $Gd(NO_3)_3{\cdot}6H_2O$ in the presence of 2-furan-carboxylic acid (fcaH) in CH_3CN results in the formation of the high-nuclearity complex $[Mn^{III}_9Mn^{II}_2Gd_2(O)_8(OH)_2(piv)_{10.6}(fca)_{6.4}(NO_3)_2(H_2O)]{\cdot}13CH_3CN{\cdot}H_2O$ [71]. The structure of the $[Mn^{III}_9Mn^{II}_2Gd_2(O)_8(OH)_2(piv)_{10.6}(fca)_{6.4}(NO_3)_2(H_2O)]$ cluster is shown in Fig. 9. The oxidation states of the manganese ions were assigned through a consideration of the coordination geometries and bond valence sum (BVS) calculations. Thus Mn(1)–Mn(9) were assigned as Mn^{III} and Mn(10) and Mn(11) as Mn^{II}. The assignments of O(10) as $(\mu_3\text{-}O)^{2-}$ and of O(2) and O(3) as $(\mu_3\text{-}OH)^-$ were also confirmed by BVS calculations and the H-atoms on O(2) and O(3) could be located and refined. The core can be described as

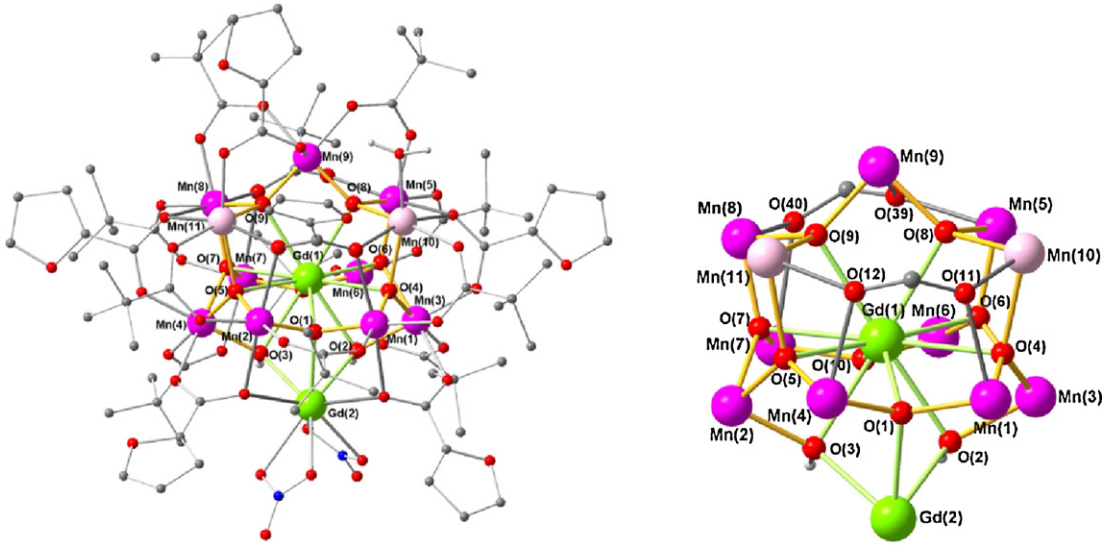

Fig. 9. Molecular structure of $[Mn^{III}_9Mn^{II}_2Gd_2(O)_8(OH)_2(piv)_{10.6}(fca)_{6.4}(NO_3)_2(H_2O)]$ (left) and its core (right). Disorder and organic H-atoms omitted for clarity Colors: Gd, green; Mn^{III}, purple; Mn^{II}, pink; O, red; N, blue; C, grey. Structural data available in Ref. [71].

bell-shaped. The Mn^{III} and Mn^{II} centers form the shell of the bell, with Mn(9) at the apex, Mn(5), Mn(8), Mn(10) and Mn(11) at the shoulder of the bell, and the remaining six Mn^{III} centers forming the rim of the bell. The two Gd centers can be thought of as forming the bell's clapper, and since the Gd···Gd vector is inclined with respect to the axis of the bell, this gives the impression that the bell is ringing. Gd(1) is 10-coordinate, and is connected to each of the 11 Mn atoms through the six (μ_4-O), one (μ_3-O) and two (μ_3-OH) bridges. Its coordination polyhedron may be best described as a bicapped square antiprism. The second Gd is nine-coordinate and hangs below the rim of the bell. It is connected to the other Gd and four of the Mn^{III} atoms through one (μ_4-O) and the two (μ_3-OH) bridges, and two oxygen atoms from two (μ_3-carboxylate) bridges. Its coordination sphere is completed by two chelating nitrate ions. The Mn centers all have octahedral coordination geometries except for Mn(6), which is square-pyramidal, with the Mn^{III} all showing the expected Jahn–Teller distortions. Of the 17 carboxylate ligands (10 pivalate, 6 furoate and 1 that is a disordered superposition), the unusual (μ_4,η^2,η^2) bridging mode is seen for one furoate and one pivalate ligand. In addition to these μ_4-bridging carboxylates, four of the furoates adopt a (μ_3,η^2,η^1) triply-bridging mode, while the sixth furoate and all the remaining pivalates form simple bridges between two metal centers. In other words, five of the six furoates bridge between three or four metal centers, whereas all but one of the pivalates adopt a simple μ-bridging mode. The Mn^{III} Jahn–Teller axes have an irregular arrangement within the aggregate core.

The *dc* magnetic susceptibility was measured at 1000 Oe in the 1.8–300 K temperature range, and showed a room temperature χT value per complex of 46.9 emu K mol^{-1}. On lowering the temperature, χT first continuously decreases reaching 35.2 emu K mol^{-1} at 37 K and then increases to a maximum value at 1.81 K of 74.5 emu K mol^{-1}. The fact that the χT product starts to saturate at 1.81 K suggests that below this temperature a well defined high spin ground state is almost exclusively thermally populated and the fit of the experimental data to a Curie–Weiss law above 30 K leads to a Curie constant of 50.8 emu K mol^{-1} and a Weiss constant of −28.1 K indicating dominant antiferro-magnetic interactions between spin carriers. The Curie constant is close to the expected value for 9 Mn^{III} ($S = 2$), 2 Mn^{II} ($S = 5/2$) and 2 Gd^{III} ($S = 7/2$) non-interacting ions (51.5 emu K mol^{-1}).

The *ac* susceptibility measurements taken over the frequency range of 1–1500 Hz and at temperatures 1.8–3 K display frequency-dependent out-of-phase signals suggesting that the complex exhibits slow relaxation of its magnetization and potential SMM behavior. In order to investigate this further, single crystal magnetization measurements were performed using an array of micro-SQUIDs at temperatures down to 40 mK. Hysteresis loops collected at varying temperatures and sweep rates (Fig. 10) show a superparamagnet-like increasing coercivity with decreasing temperature confirming the compound to be a SMM. No steps due to quantum tunneling of magnetization (QTM) were observed, probably as a result of ligand and lattice solvent disorder, as there are no obvious pathways for intermolecular interactions. *dc* magnetization decay data were collected in the 0.04–1.0 K range: at each temperature, the magnetization was saturated with a *dc* field, the temperature lowered to a chosen value, the field switched off, and the decay monitored with time. The data were scaled in a single master curve in order to construct the Arrhenius plot and the fit of the thermally activated region above ~0.5 K gave $\tau_0 = 2 \times 10^{-12}$ s and an effective barrier $\Delta E/k_B = 18.4$ K which was the highest value reported at this time for 3d–4f SMMs [71]. Given the lack of obvious intermolecular interactions, the relatively low value of τ_0 compared with other 3d–4f SMMs might be the result of the presence of a higher spin state. Below ~0.16 K, the relaxation time becomes essentially temperature-independent, consistent with the purely quantum regime where QTM is only via the lowest energy $\pm m_S$ levels. Probably the Jahn–Teller distortions of the Mn^{III} centers make the major contribution to the anisotropy with the Mn^{II} and Gd^{III} centers contributing to the spin.

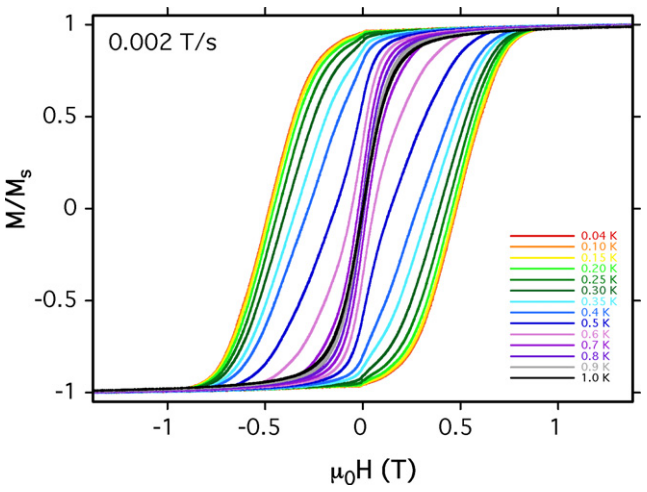

Fig. 10. Magnetization (M) vs. applied *dc* field ($\mu_0 H$) for $[Mn^{III}_9Mn^{II}_2Gd_2(O)_8(OH)_2(piv)_{10.6}(fca)_{6.4}(NO_3)_2(H_2O)]\cdot 13CH_3CNH_2O$. Data from Ref. [71].

3.1.3. Site-targeted reactions

Selective replacement of components of 3d–4f clusters has been identified as a promising way of studying how the different electronic structures and properties of the 3d and 4f ions can contribute to single molecule magnet behavior. Compounds containing lanthanide ions often have the useful property that they form isostructures for given groups of 4f ions. It is possible to produce 3d–4f systems using assisted self assembly reactions where we can then choose to vary the 3d or 4f site, for example, replacing isotropic Fe^{III} with anisotropic Mn^{III} to study the effect on magnetic behavior with a variety of 4f ions. It is often the case that the larger lanthanide ions to the left of the series form one structural type whereas those to the right form a different structure. Thus, it was possible to produce the Mn^{III} analogues of the $[Fe^{III}_5Ln_8(\mu_3\text{-}OH)_{12}(L)_4(piv)_{12}(NO_3)_4(OAc)_4]^-$ described above but using ^{t}Bu-*N*-diethanolamine in place of ^{n}Bu-*N*-diethanolamine [72]. Indeed, for the Mn^{III} series it proves possible to crystallize examples further to the right in the lanthanide series up to the (often magnetically more interesting) Tb^{III} analogue. We found the Pr^{III} and Nd^{III} compounds have dominant antiferro-magnetic interactions, the Sm^{III} compound is paramagnetic and the Gd^{III} and Tb^{III} compounds are ferromagnetically coupled with large spin ground states. However, although the Tb analogue also shows a significant anisotropy, we could not observe any slow relaxation of the magnetization, at least above 1.8 K.

This general approach did, however, lead to a series of SMMs when the diethanolamine ligand was changed to *N*-methyldiethanolamine [49]. Here we can illustrate how selective replacement of the lanthanide ions in a $[Mn_5Ln_4]$ SMM system forming with the smaller radius Ln^{III} ions can be used to establish the influences of the individual components on SMM behavior. The assisted self assembly reaction of $[Mn_6O_2(Piv)_{10}(4\text{-}Me\text{-}py)_{2.5}(PivH)_{1.5}]$ with *N*-methyldiethanolamine ($mdeaH_2$) and $Ln(NO_3)_3\cdot 6H_2O$ leads to the formation of isostructural crystals of $[Mn_5Ln_4(O)_6(mdea)_2(mdeaH)_2(Piv)_6(NO_3)_4(H_2O)_2]\cdot 2MeCN$. By using Ln^{3+} = Tb, Dy, Ho and Y it is possible to vary the contribution of Ln to the overall electronic structure of the system in a targeted fashion [49]. The rare earth ion Y^{3+} has an ionic radius of similar size to that of Ho^{3+}, but is, of course, diamagnetic. In this way, it was possible to compare the magnetic behavior for an isostructural

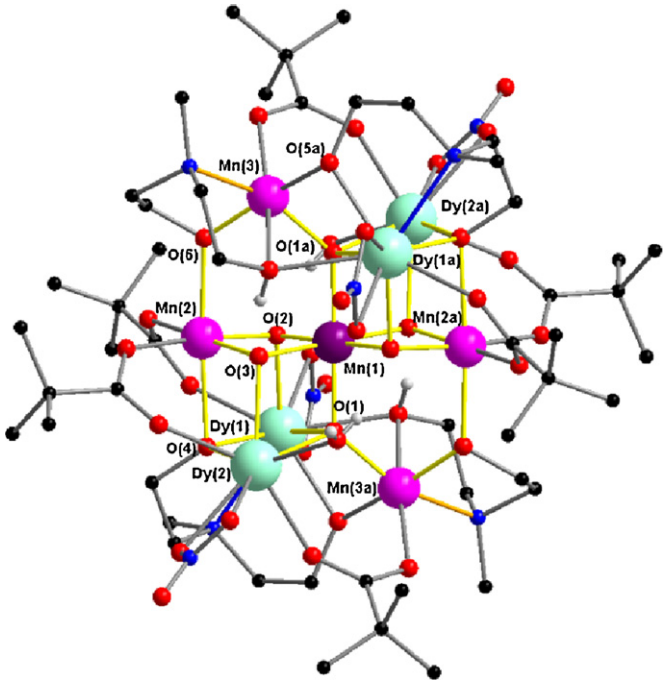

Fig. 11. Structure of $[Mn_5Dy_4(O)_6(mdea)_2(mdeaH)_2(piv)_6(NO_3)_4(H_2O)_2]$. Structural data available in Ref. [49].

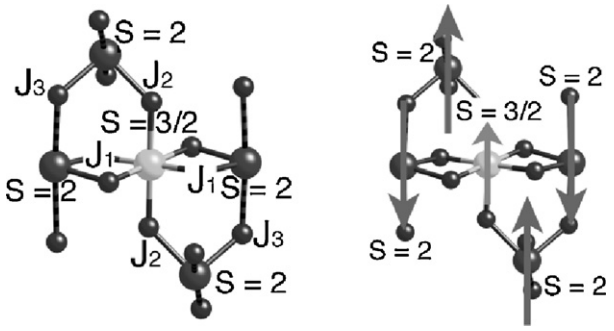

Scheme 2. Topology of the intra-complex magnetic interactions for the $[Mn_5Y_4]$ derivative.

series of compounds where the contribution from the Ln could be completely switched off.

The molecular structure (Fig. 11) consists of a centrosymmetric $\{Mn_5Ln_4\}^{28+}$ core, held together by four $(\mu_3\text{-}O)^{2-}$ and two $(\mu_4\text{-}O)^{2-}$ ligands, and the oxygen atoms of two monodeprotonated $\eta^2{:}\eta^2{:}\eta^1{:}\mu^3$- and two doubly-deprotonated $\eta^3{:}\eta^2{:}\eta^1{:}\mu^4$-diethanolamine ligands. The structure is further described for the Dy analogue. Peripheral ligation is provided by six μ-pivalate anions, four nitrate anions (one chelating each Ln ion) and a water molecule on each of Dy(2) and Dy(2a). The metal oxidation states (Mn^{III}, Mn^{IV}, Dy^{III}) and the deprotonation levels of O^{2-}, $mdea^{2-}$ and $mdeaH^-$ ions were established by charge considerations, bond valence sum calculations, inspection of metric parameters and the observation of Jahn–Teller elongation axes of Mn^{III}. All five Mn atoms are six-coordinate. Dy(1) is nine-coordinate with a coordination polyhedron that may best be described as a triaugmented triangular prism, while Dy(2) is eight-coordinate and the coordination polyhedron could be described as between a distorted bicapped trigonal prism and a square antiprism. Inspection of the central core reveals two distorted $\{Mn^{IV}Mn^{III}Dy_2O_4\}$ cubanes sharing a Mn^{IV} vertex, Mn(1). One oxo ligand in each cubane, O(1), bridges to a further Mn^{III} center, Mn(3), which is further linked to Mn(2) and two Dy centers in the dicubane core by diethanolamine oxygen atoms. The monodeprotonated $mdeaH^-$ groups act as tridentate chelates on each of the outer Mn (Mn(3), Mn(3a)) atoms, while the two doubly deprotonated $mdea^{2-}$ anions each chelate about a Dy center, Dy(2). The Mn^{III} ions have the expected octahedral geometries with Jahn–Teller elongations along one axis, while Mn^{IV} has a rather symmetric octahedral geometry.

The magnetic properties of all the complexes were studied. In the Y^{III} compound the rare earth ions are diamagnetic allowing us to study independently the magnetism of the $Mn^{III}_4Mn^{IV}$ unit. When the temperature is lowered at a field of 0.1 T, the χT product decreases to a minimum value of 1.8 emu K mol^{-1} at 1.8 K. Based on the structure of the compound, the χT product was simulated taking into account only three isotropic intra-complex magnetic interactions as shown in Scheme 2 and neglecting the low temperature data (below 10 K) to avoid additional effects coming from the magnetic anisotropy and/or weak inter-complex interactions. The following spin Heisenberg Hamiltonian was thus considered:

$$H = -J_1S_5(S_1 + S_3) - J_2S_5(S_2 + S_4) - J_3(S_1S_2 + S_3S_4) \quad (5)$$

where J_1, J_2 and J_3 are the exchange interactions between Mn^{III} and Mn^{IV} sites through double O bridges between Mn^{III} and Mn^{IV} ions, through single O bridges, and between Mn^{III} ions through single alkoxo bridges, respectively, and S_i the spin vectors for each of the metal ions ($S_i = 2$ for Mn^{III} with $i = 1$–4 and $S_5 = 3/2$ for Mn^{IV}). The simulation of the experimental data above 10 K gave $J_1/k_B = -90(4)$ K, $J_2/k_B = +12(1)$ K, $J_3/k_B = -18(1)$ K and $g = 2.1(1)$. Therefore even if ferromagnetic interactions are present between Mn^{III} and Mn^{IV}, the AF interactions dominate and lead to a global decrease of the χT product at high temperature as is observed experimentally for all the compounds. This set of magnetic interactions induces an

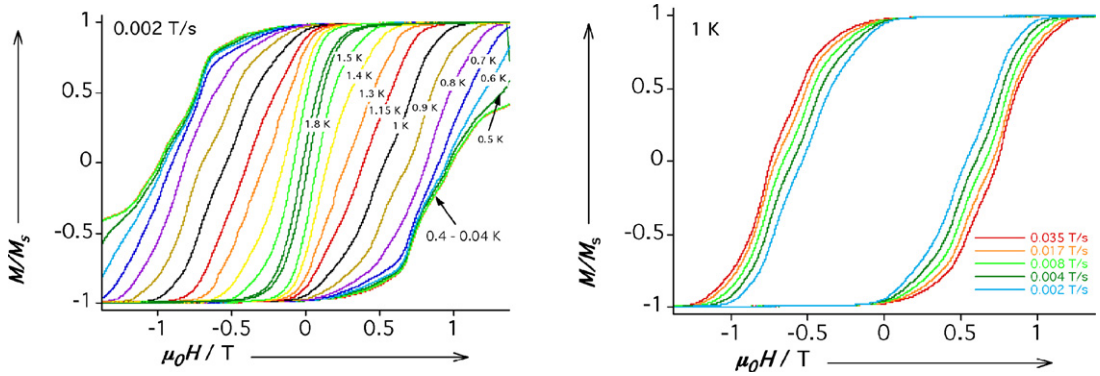

Fig. 12. Field dependence of the magnetization measured in the easy direction of a single crystal of $[Mn_5Dy_4]$. The temperature dependence at a fixed scan rate of 2 mT/s (left); the scan-rate dependence at a fixed temperature of 1.0 K (right). Redrawn from Ref. [49].

$S_T = 3/2$ ground state with the spin topology given in Scheme 2. At 1.85 K, M vs. H measurements revealed a lack of a true saturation even at 70 kOe at which M reaches 2.7 μ_B in good agreement with an $S_T = 3/2$ ground state. The slow saturation of the magnetization confirms also the presence of a significant anisotropy as expected in presence of Mn^{III} metals ions.

By studying the dynamics of the relaxation of the magnetization for all compounds, it was possible to estimate barrier heights for each. Thus, the $[Mn_5Y_4]$ compound has an energy gap of 20.2 K while the "best" of the SMMs was $[Mn_5Dy_4]$ with an almost doubled gap of 38.6 K. This compound shows a nice hysteresis behavior which is already visible at 1.8 K (Fig. 12). Currently this is the highest barrier recorded for 3d–4f systems and suggests promising ways forward in introducing rare earth anisotropy into SMM systems.

4. Pure 4f polynuclear systems

We have already mentioned the exciting results obtained in phthalocyanine-based single ion SMM comprising Tb, Dy, and Ho. From a chemical point of view the oxidation of $[M(Pc)_2]^-$ to the neutral state has provided a further increase in the blocking temperature [8]. More recently it has been reported that polyoxometalates (POMs) are able to encapsulate lanthanides with coordination geometries similar to those of bis(phthalocyaninato)lanthanide complexes to give the polyanion $[ErW_{10}O_{36}]^{9-}$. Frequency dependent χ'' has been observed below 8 K in the sodium salt [73].

A few reports have appeared to date on purely lanthanide-based polynuclear systems [74,75]. An interesting example is $Dy_{10}(OC_2H_4OCH_3)_{30}$ [76], which shows a regular ring structure similar to that of the "ferric wheel" [77]. The record in the nuclearity has been later surpassed in a dodecalanthanide wheel supported by calix[4]arene ligands [78]. Among the smaller complexes triangular clusters have received a deal of great attention, as discussed in detail in the following section.

4.1. Spin chirality in a Dy_3 triangle

The strong Ising anisotropy of some lanthanides combined with spin non-collinearity typical of molecule-based magnetic materials is at the basis of the exotic properties of a triangular Dy^{III} cluster based on the use of the *ortho*-vanillin ligand, of formula $[Dy_3(OH)_2(o\text{-van})_3(H_2O)_5Cl]^{3+}$, Dy_3, whose structure is shown in Fig. 13 [79].

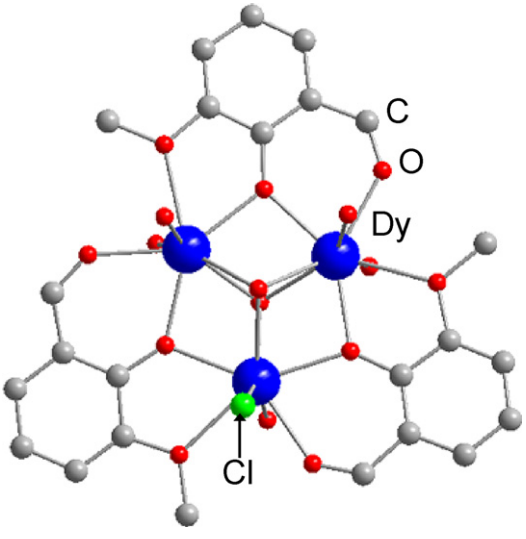

Fig. 13. View of the structure of the $[Dy_3(OH)_2(o\text{-van})_3(H_2O)_5Cl]^{3+}$ cation. Crystallographic data available in Ref. [79].

The three lanthanide ions are held together by a multiple bridging constituted by five oxygen atoms, two belonging to the OH^- ions lying above and below the plane of the triangle and the other three to the phenolato group of the *o*-vanillin ligands. The axial positions, referring to the Dy_3 plane, are occupied by five water molecules and one chloride ion. The remaining anions are not coordinated but connected through a network of hydrogen bonds.

The *o*-vanillin ligand was first used by Costes et al. with Gd^{III} ions and an almost isostructural triangular cluster was obtained [80]. In the case of isotropic Gd^{III} the magnetic behavior is characterized by antiferro-magnetic interaction, $J/k_B = -0.095$ K, between the $S = 7/2$ spins of Gd^{III}. The ground state in a triangle of half-integer spins antiferro-magnetically coupled has $S_T = 1/2$ but, as a result of spin frustration effects and the weak value of the exchange interaction, a monotonic decrease of the χT product on lowering the temperature was observed without selective thermal population of the ground state.

The magnetic properties of the Dy^{III} analogue revealed the presence of antiferro-magnetic interaction, but, rather surprisingly, the magnetic susceptibility shows a maximum around $T = 7$ K, as shown in Fig. 14, suggesting the presence of a non-magnetic ground state. This was confirmed also by the magnetization curve at low temperature, shown in Fig. 14, which remains practically flat at almost zero magnetization for low fields with a sudden jump to the saturation value of 20 μ_B around 8 kOe [79].

Using the assumption for Dy^{III} of an effective $S_{eff} = 1/2$ with large easy axis anisotropy, i.e. the magnetic moment is represented by an arrow lying along the easy axis with only the up and down configurations available, two limiting cases can be expected, as illustrated in Fig. 15, depending on the orientation of the local easy axes.

If the anisotropy axes point perpendicular to the plane of the triangle, the typical spin frustrated situation is encountered. The ground state is, however, magnetic and the application of a strong enough magnetic field overcoming the antiferro-magnetic interaction leads to a step in the magnetization from the value of $(1/3)M_S$ to full saturation, M_S. This is clearly not the case for Dy_3. The only way of observing a non-magnetic ground state in a system comprising an odd number of unpaired electrons is that the magnetic anisotropy forces the magnetic moment to lie in the plane of the triangle. As a result of the C_3 symmetry the magnetic moments are not collinear but at 120° to each other and the resultant is zero. Assuming the presence of a strong magnetic anisotropy that forces the magnetic moment to lie in the plane, the application of a magnetic field out of the plane has a negligible effect. On the contrary, when the magnetic field is applied in the plane of the triangle, it polarizes all the magnetic moments without deviating them from their easy axis, thus leading suddenly to saturation. Parallel alignment of the magnetic moments could only be reached using exceedingly strong magnetic fields capable of overcoming the Dy^{III} magnetic anisotropy. This interesting picture of a toroidal arrangement of the spins has been simultaneously and independently confirmed by single-crystal magnetic measurements [81] and ab initio calculations [82], which have revealed Dy_3 as a unique system showing the phenomenon of spin chirality. Ab initio calculations, based on the complete active space self-consistent-field (CASSCF) method, have shown that each Dy^{III} in the triangle has a ground state doublet mainly described as $|J = 15/2, m_J = \pm 15/2>$. The first excited doublet is separated by ca. 200–300 K, depending on which of the three non-equivalent sites is considered. The method allows one to extract both the **g** tensor associated to the ground doublet, thus treated as an effective $S_{eff} = 1/2$, and its spatial orientation. The **g** tensor for the three Dy^{III} ions is Ising-like and very anisotropic, $g_z \cong 19.8$ and $g_{x,y}$ not exceeding 0.1. An effective gyromagnetic factor of 20 is expected if the ground doublet for the Dy^{III} ions is well described by $|J = 15/2, m_J = \pm 15/2>$ being $g_{J=15/2} = 4/3$. The local z axes are close to the Dy_3 plane (deviations ranging from −4.3° to 8.8°) [82]. These

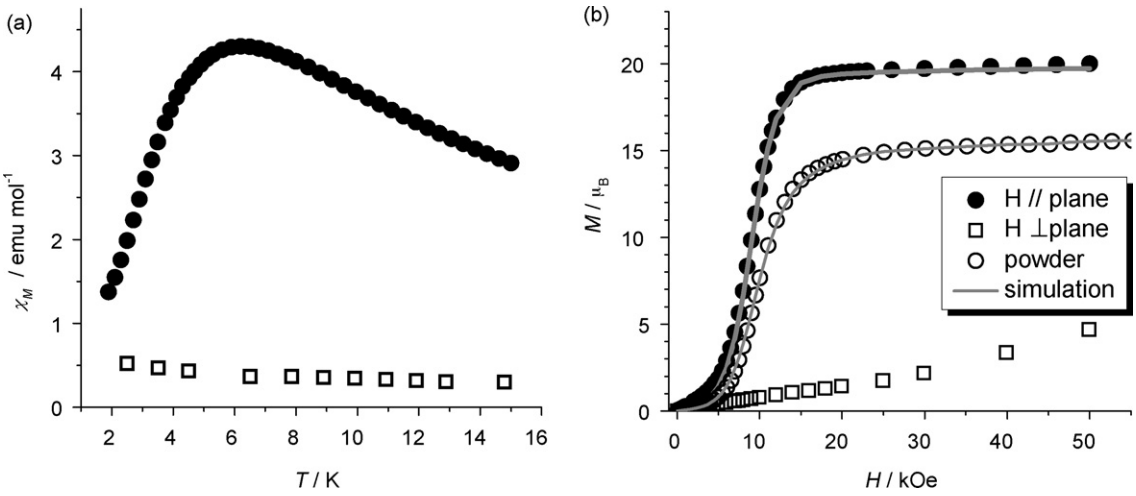

Fig. 14. (a) Temperature dependence of the magnetic susceptibility of a single crystal of Dy_3 measured with the field applied in the Dy_3 plane, solid circles, and perpendicular to it (empty squares). (b) Field dependence of the magnetization at $T = 1.9$ K, measured with the field applied in the Dy_3 plane (solid circles), perpendicular to it (empty squares), or to a polycrystalline powder pressed in a pellet to avoid orientation of the crystallites (empty circles). The solid line represents the best fit curves obtained with a non-collinear Ising model. Redrawn from data of Ref. [81].

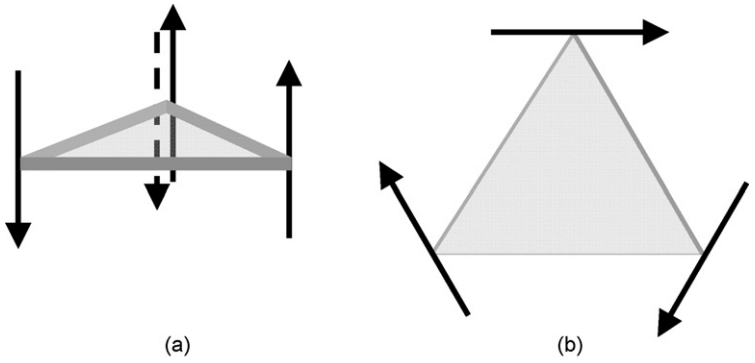

Fig. 15. Schematic view of the arrangement of three Ising spins in a triangle in the two limiting cases; (a) the easy axes point perpendicular to the plane of the triangle and spin frustration is observed; (b) the easy axes lie in the plane of the triangle with no resultant magnetic moment.

results nicely agree with the information extracted from the simulation of single crystal magnetic data [81]. More recently the same theoretical approach has been used to rationalize angular dependent magnetic data of Dy complexes with NIT-R radicals, either in monomeric [83] or chain structures [84], and demonstrated to correctly predict the orientation of the easy axis of Dy ions also in low symmetry environments.

It is interesting to focus on the energy level scheme of the 2^3 states originating from the interaction of the ground doublets of the three Dy^{III} ions, which can be calculated in the simplified scheme of a pure Ising Hamiltonian:

$$H = -\sum_{i,k=1,2,3(i>k)} j_{zz} S_{z_i} S_{z_k} - \mu_B \sum_{i=1,2,3} g_z H_{z_i} S_{z_i} \quad (6)$$

where the z_i refers to the local easy axis of site i. The simultaneous fitting of the M vs. H and χ vs. T data has provided for Dy_3 $j_{zz}/k_B = 10.6(4)$ K and $g_z = 20.7(1)$, this last value in nice agreement with ab initio calculations. The large value of j_{zz}/k_B, compared to that observed in Gd_3 [80], is again due to the use of a $S_{eff} = 1/2$. In fact the exchange energy JS^2 is 2.65 and 1.16 K for Dy_3 and Gd_3, respectively. Indeed in a more complex treatment, which takes into account the first two doublets of the $J = 15/2$ manifold and $g_J = 4/3$, the coupling constant reduces to $-0.092(2)$ K.

In Fig. 16 the Zeeman splitting of the lowest eight states when the field is applied along one of the local easy axis is shown. A non-magnetic doublet is separated by ca. 11 K from the remaining 6

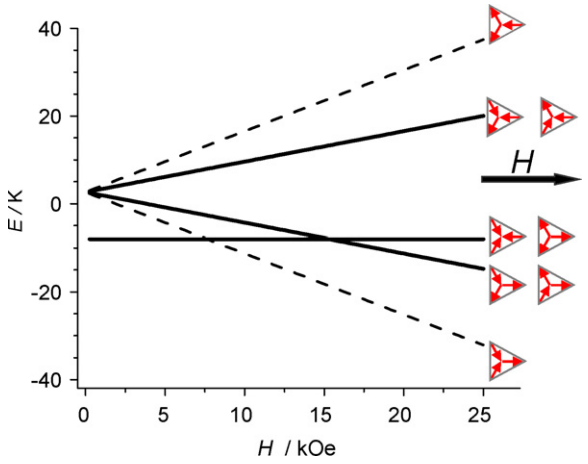

Fig. 16. Zeeman splitting of the 8 states originating from the Ising interaction of three effective spins $S_{eff} = 1/2$ with easy axes lying in the plane of the triangle. The magnetic field is applied along the easy axis of one of the three spins. The solid lines represent for doubly degenerate states. The orientation of the arrows on the left describes the spin structure of the state. The parameters used for the calculation are those obtained from the best fit of the magnetic data of Dy_3.

which are degenerate in zero field. The two states of the ground doublet are, however, distinguished by a different chirality, as the spins are oriented either clock- or anticlock-wise. The application of the field in the plane splits the degeneracy of the six remaining states. In particular, if the field is applied along one of the easy axis the six manifold splits in two type of states, those where all moments have either a positive or negative component along the field, and the second set, double degenerate, where only two moments have positive (negative) projection along the field. The more magnetic of these states becomes the ground one for fields stronger than the crossing field, H_C = 8 kOe. At this field, a jump in the magnetization to saturation is in fact experimentally observed.

The behavior observed in Dy_3 is not generally found for a triangular cluster. In fact a triangular Dy_3 unit, with the edges decorated by pairs of antiferro-magnetically coupled copper(II) ions to yield the compound of formula $[Dy_3Cu_6L_6(OH)_6(H_2O)_{10}]^{3+}$, where H_2L is the Schiff base 1,1,1-trifluoro-7-hydroxy-4-methyl-5-azahept-3-en-2-one [42], has been recently reported. In this case the magnetization vs. field curves show a rapid saturation to $(1/3)M_S$ and then a jump to full saturation around H = 20 kOe. This case is consistent with the spin arrangement described in Fig. 15a.

Dy_3 appears therefore to be the archetype of the non-collinear Ising model but its interesting features are not limited to the static magnetic properties. If investigated with *ac* susceptibility, Dy_3 reveals a frequency dependence of both χ' and χ'' [79]. By plotting χ'' vs. the applied frequency it has been possible to extract the relaxation time which increases on lowering the temperature down to ca. 7 K, with a very small energy barrier, ca. 36 K. Below 8 K, strong deviations from the Arrhenius law are observed with a reduction of the slope. Given that the ground state of Dy_3 is essentially non-magnetic, the dynamics we observe seem to be associated with the excited states, a fully unprecedented phenomenon in molecular magnetism. Interestingly the application of a static field strongly reduces the relaxation rate and in a magnetic field the barrier increases up to ca. 120 K. The condition for which an additional underbarrier pathway for the reversal of the magnetization is accessible is suddenly re-established at the level crossing field, where a steep increase of the relaxation rate is observed as shown in Fig. 17. Quantum effects, due to the possibility of level admixing are therefore observed in Dy_3, as well as in other Dy-based SMMs [62,85,86], despite the classical nature of the Ising model.

Triangular clusters have been intensively investigated in the past to explore the rich physics related to spin frustration. More recently triangles of S = 1/2, e.g. copper(II) ions, have been proposed as qubits that can be controlled through electric fields [87]. The case of Dy_3 is, however, unique. The Ising nature of the ions reduces the quantum nature of the system but introduces other interesting features. Dy_3 can in fact be seen as a system of three single ion SMMs weakly interacting. The relaxation we have monitored with *ac* susceptometry corresponds mainly to the reversal of one Dy^{III} at a time, while the transition from one state of the non-magnetic ground doublet to the other requires the reversal of all the three magnetic moments at the same time. This is a very unlikely event and a much longer characteristic time is expected. It could therefore be possible to store the information in the spin chirality of the triangular unit even if the system has no net magnetic moment, with the advantage of much weaker dipolar fields and a reduced sensitivity to external fields. However, the transition between the two chiral states cannot be monitored with standard magnetometry but only with local probes, like NMR or muon spin resonance techniques.

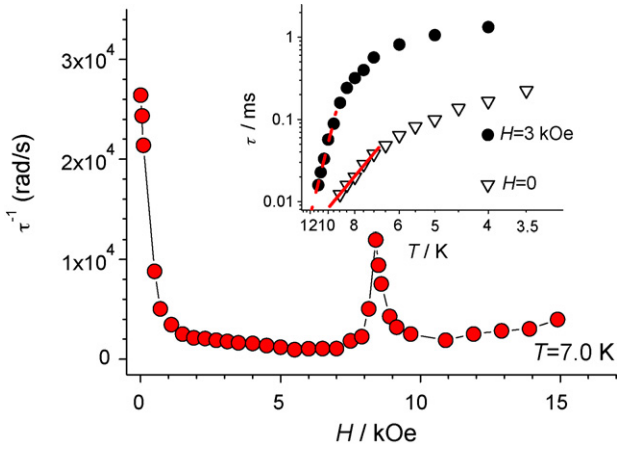

Fig. 17. Field dependence of the relaxation rate of Dy_3 as extracted from *ac* susceptibility data. The field is applied in the plane of the triangle. In the inset the temperature dependence of the relaxation time is shown in the Arrhenius plot for zero static field and for a static field where tunneling is suppressed. Redrawn from data of Ref. [81].

5. Conclusions

While not intending to review exhaustively the results obtained in the very active and promising field of single molecule magnets based on lanthanide ions, we hope to have provided here an interesting example of concerted actions in the synthesis and characterization of lanthanide-based molecular nanomagnets.

Notwithstanding the unavoidable drawbacks related to the inherently weak magnetic exchange interactions, lanthanides present appealing features. Isotropic ions, like Gd^{III}, can contribute to increase the spin of the ground state of 3d–4f clusters thanks to the ferromagnetic interactions often present in compounds containing this ion. In this case the necessary magnetic anisotropy is provided by the 3d metal ions. On the contrary, anisotropic lanthanide ions can be combined with almost isotropic metal ions to amplify the exchange interaction. The possibility to obtain isostructural systems with diamagnetic Y^{III} ions has also contributed to elucidating the mechanism of exchange interaction and slow relaxation in these systems. Last, but not least, the presence of a strong anisotropy which exceeds the magnetic exchange interaction leads to a scenario for slow relaxation that is significantly different from that of 3d-based SMMs, opening the perspective of a fully unprecedented type of magnetic memory, where the information is stored in the chirality of the spin arrangement without any net magnetic moment.

Acknowledgments

The financial support of the Deutsche Forschungsgemeinschaft thanks to the Schwerpunktptprogramm Molekularer Magnetismus (SPP1137) has been key for the development of this coordinated work. We mourn the premature passing away of Dr. Karlheinz Schmidt, whose passionate supervision of the program promoted the development and integration of the molecular magnetism community.

The results reviewed here have of course been obtained thanks to the outstanding contribution of other scientists, some of them having benefited from a DFG fellowship. We thank Olivier Cador, Patrick Rosa, Guillaume Chastanet, Fabrice Pointillart, Kevin Bernot, Lapo Bogani, Giordano Poneti, Cristiano Benelli, Ayuk Ako, Valeriu Mereacre, Jinkui Tang, Madhu Thomas, Yanhua Lan, Christopher Anson, Gang Wu, Ian Hewitt, Rodolphe Clérac, and Wolfgang Wernsdorfer.

References

[1] A. Abragam, B. Bleaney, Electron Paramagnetic Resonance of Transition Ions, Dover, New York, 1986.
[2] D. Gatteschi, R. Sessoli, J. Villain, Molecular Nanomagnets, Oxford University Press, Oxford, UK, 2006.

[3] N. Ishikawa, M. Sugita, T. Ishikawa, S. Koshihara, Y. Kaizu, J. Am. Chem. Soc. 125 (2003) 8694.
[4] L.J.F. Broer, C.J. Gorter, Physica X (1943) 621.
[5] C.J. Gorter, Paramagnetic Relaxation, Elsevier, Amsterdam, 1947.
[6] A.H. Morrish, The Physical Principles of Magnetism, John Wiley & Sons, Inc., New York, 1966.
[7] N. Ishikawa, M. Sugita, T. Okubo, N. Tanaka, T. Lino, Y. Kaizu, Inorg. Chem. 42 (2003) 2440.
[8] N. Ishikawa, M. Sugita, N. Tanaka, T. Ishikawa, S.Y. Koshihara, Y. Kaizu, Inorg. Chem. 43 (2004) 5498.
[9] N. Ishikawa, Polyhedron 26 (2007) 2147.
[10] D. Luneau, P. Rey, Coord. Chem. Rev. 249 (2005) 2591.
[11] J.C.G. Bunzli, C. Piguet, Chem. Soc. Rev. 34 (2005) 1048.
[12] J.C.G. Bunzli, C. Piguet, Chem. Rev. 102 (2002) 1897.
[13] C. Benelli, D. Gatteschi, Chem. Rev. 102 (2002) 2369.
[14] X.H. Zhang, S.T. Yang, S.P. Wang, Prog. Chem. 20 (2008) 1073.
[15] A. Caneschi, D. Gatteschi, R. Sessoli, P. Rey, Acc. Chem. Res. 22 (1989) 392.
[16] C. Benelli, A. Caneschi, D. Gatteschi, L. Pardi, P. Rey, Inorg. Chem. 28 (1989) 275.
[17] C. Benelli, D. Gatteschi, R. Sessoli, A. Rettori, M.G. Pini, F. Bartolome, J. Bartolome, J. Magn. Magn. Mater. 140 (1995) 1649.
[18] F. Cinti, A. Rettori, M.G. Pini, M. Mariani, E. Micotti, A. Lascialfari, N. Papinutto, A. Amato, A. Caneschi, D. Gatteschi, M. Affronte, Phys. Rev. Lett. 100 (2008) (art. no. 057203).
[19] F. Cinti, A. Rettori, M. Barucci, E. Olivieri, L. Risegari, G. Ventura, A. Caneschi, D. Gatteschi, D. Rovai, M.G. Pini, M. Affronte, M. Mariani, A. Lascialfari, J. Magn. Magn. Mater. 310 (2007) 1460.
[20] C. Benelli, A. Caneschi, D. Gatteschi, R. Sessoli, J. Appl. Phys. 73 (1993) 5333.
[21] C. Benelli, A. Caneschi, D. Gatteschi, R. Sessoli, Inorg. Chem. 32 (1993) 4797.
[22] C. Benelli, A. Caneschi, D. Gatteschi, R. Sessoli, Adv. Mater. 4 (1992) 504.
[23] K. Bernot, L. Bogani, A. Caneschi, D. Gatteschi, R. Sessoli, J. Am. Chem. Soc. 128 (2006) 7947.
[24] L. Bogani, C. Sangregorio, R. Sessoli, D. Gatteschi, Angew. Chem. Int. Ed. 44 (2005) 5817.
[25] A. Caneschi, D. Gatteschi, N. Lalioti, C. Sangregorio, R. Sessoli, G. Venturi, A. Vindigni, A. Rettori, M.G. Pini, M.A. Novak, Angew. Chem. Int. Ed. 40 (2001) 1760.
[26] R. Clerac, H. Miyasaka, M. Yamashita, C. Coulon, J. Am. Chem. Soc. 124 (2002) 12837.
[27] C. Coulon, H. Miyasaka, R. Clérac, Struct. Bond 122 (2006) 163.
[28] L. Bogani, A. Vindigni, R. Sessoli, D. Gatteschi, J. Mater. Chem. 18 (2008) 4750.
[29] G. Poneti, K. Bernot, L. Bogani, A. Caneschi, R. Sessoli, W. Wernsdorfer, D. Gatteschi, Chem. Commun. (2007) 1807.
[30] C. Benelli, A. Caneschi, D. Gatteschi, L. Pardi, Inorg. Chem. 31 (1992) 741.
[31] W. Wernsdorfer, Adv. Chem. Phys. 118 (2001) 99.
[32] L. Bogani, A. Caneschi, M. Fedi, D. Gatteschi, M. Massi, M.A. Novak, M.G. Pini, A. Rettori, R. Sessoli, A. Vindigni, Phys. Rev. Lett. 92 (2004) (art. no. 207204).
[33] M. Andruh, O. Kahn, J. Sainton, Y. Dromzee, S. Jeannin, Inorg. Chem. 32 (1993) 1623.
[34] J.P. Costes, F. Dahan, A. Dupuis, Inorg. Chem. 39 (2000) 5994.
[35] F. Pointillart, K. Bernot, R. Sessoli, Inorg. Chem. Commun. 10 (2007) 471.
[36] S. Osa, T. Kido, N. Matsumoto, N. Re, A. Pochaba, J. Mrozinski, J. Am. Chem. Soc. 126 (2004) 420.
[37] A. Mishra, W. Wernsdorfer, K.A. Abboud, G. Christou, J. Am. Chem. Soc. 126 (2004) 15648.
[38] C.M. Zaleski, E.C. Depperman, J.W. Kampf, M.L. Kirk, V.L. Pecoraro, Angew. Chem. Int. Ed. 43 (2004) 3912.
[39] F. Mori, T. Ishida, T. Nogami, Polyhedron 24 (2005) 2588.
[40] J.P. Costes, F. Dahan, W. Wernsdorfer, Inorg. Chem. 45 (2006) 5.
[41] S. Ueki, T. Nogami, T. Ishida, M. Tamura, Mol. Cryst. Liquid Cryst. 455 (2006) 129.
[42] C. Aronica, G. Pilet, G. Chastanet, W. Wernsdorfer, J.F. Jacquot, D. Luneau, Angew. Chem. Int. Ed. 45 (2006) 4659.
[43] T. Hamamatsu, K. Yabe, M. Towatari, S. Osa, N. Matsumoto, N. Re, A. Pochaba, J. Mrozinski, J.L. Gallani, A. Barla, P. Imperia, C. Paulsen, J.P. Kappler, Inorg. Chem. 46 (2007) 4458.
[44] S. Ueki, A. Okazawa, T. Ishida, T. Nogami, H. Nojiri, Polyhedron 26 (2007) 1970.
[45] S. Ueki, T. Ishida, T. Nogami, K.Y. Choi, H. Nojiri, Chem. Phys. Lett. 440 (2007) 263.
[46] C.M. Zaleski, J.W. Kampf, T. Mallah, M.L. Kirk, V.L. Pecoraro, Inorg. Chem. 46 (2007) 1954.
[47] V. Mereacre, D. Prodius, A.M. Ako, N. Kaur, J. Lipkowski, C. Simmons, N. Dalal, I. Geru, C.E. Anson, A.K. Powell, C. Turta, Polyhedron 27 (2008) 2459.
[48] T. Yamaguchi, Y. Sunatsuki, H. Ishida, M. Kojima, H. Akashi, N. Re, N. Matsumoto, A. Pochaba, J. Mrozinski, Inorg. Chem. 47 (2008) 5736.
[49] V. Mereacre, A.M. Ako, R. Clerac, W. Wernsdorfer, I.J. Hewitt, C.E. Anson, A.K. Powell, Chem. Eur. J. 14 (2008) 3577.
[50] G. Novitchi, J.P. Costes, J.P. Tuchagues, L. Vendier, W. Wernsdorfer, New J. Chem. 32 (2008) 197.
[51] G. Wu, I.J. Hewitt, S. Mameri, Y. Lan, R. Clerac, C.E. Anson, S. Qiu, A.K. Powell, Inorg. Chem. 46 (2007) 7229.
[52] (a) R. Sreenivasulu, J. Sreeramulu, Acta Cien. Ind. Chem. 30 (2004) 181;
(b) S.C. Rustagi, G.N. Rao, Indian J. Chem. 13 (1975) 702;
(c) G. Asgedom, A. Sreedhara, C.P. Rao, Polyhedron 14 (1995) 1873;
(d) M. Dey, C.P. Rao, P.K. Saarenketo, K. Rissanen, E. Kolehmainen, Eur. J. Inorg. Chem. 8 (2002) 2207;
(e) M. Dey, C.P. Rao, P.K. Saarenketo, K. Rissanen, Inorg. Chem. Commun. 5 (2002) 924.
[53] D. Marcos, J.V. Folgado, D. Beltran-Porter, M.T. Do Prado-Gambardella, S.H. Pulcinelli, R.H. De Almeida-Santos, Polyhedron 9 (1990) 2699.
[54] M. Ferbinteanu, T. Kajiwara, K.Y. Choi, H. Nojiri, A. Nakamoto, N. Kojima, F. Cimpoesu, Y. Fujimura, S. Takaishi, M. Yamashita, J. Am. Chem. Soc. 128 (2006) 9008.
[55] T. Kajiwara, R. Sensui, T. Noguchi, A. Kamiyama, T. Ito, Inorg. Chim. Acta 337 (2002) 299.
[56] A. Kamiyama, T. Noguchi, T. Kajiwara, T. Ito, Inorg. Chem. 41 (2002) 507.
[57] A. Kamiyama, T. Noguchi, T. Kajiwara, T. Ito, Cryst. Eng. Commun. 5 (2003) 231.
[58] T. Kajiwara, M. Nakano, Y. Kaneko, S. Takaishi, T. Ito, M. Yamashita, A. Igashira-Kamiyama, H. Nojiri, Y. Ono, N. Kojima, J. Am. Chem. Soc. 127 (2005) 10150.
[59] A.M. Madalan, K. Bernot, F. Pointillart, M. Andruh, A. Caneschi, Eur. J. Inorg. Chem. (2007) 5533.
[60] A. Kamiyama, T. Noguchi, T. Kajiwara, T. Ito, Angew. Chem. Int. Ed. 39 (2000) 3130.
[61] F. Pointillart, K. Bernot, R. Sessoli, D. Gatteschi, Chem. Eur. J. 13 (2007) 1602.
[62] F. Mori, T. Nyui, T. Ishida, T. Nogami, K.Y. Choi, H. Nojiri, J. Am. Chem. Soc. 128 (2006) 1440.
[63] C. Dekker, A.F.M. Arts, H.W. Wijn, A.J. van Duyneveldt, J.A. Mydosh, Phys. Rev. B 40 (1989) 11243.
[64] K.S. Cole, R.H. Cole, J. Chem. Phys. 9 (1941) 341.
[65] A.L. Barra, A. Caneschi, A. Cornia, D. Gatteschi, L. Gorini, L.P. Heiniger, R. Sessoli, L. Sorace, J. Am. Chem. Soc. 129 (2007) 10754.
[66] K. Bernot, J. Luzon, R. Sessoli, A. Vindigni, J. Thion, S. Richeter, D. Leclercq, J. Larionova, A. Van Der Lee, J. Am. Chem. Soc. 130 (2008) 1619.
[67] (a) G. Christou, Acc. Chem. Res. 22 (1989) 328;
(b) G. Christou, Polyhedron 24 (2005) 2065.
[68] M. Murugesu, A. Mishra, W. Wernsdorfer, K.A. Abboud, G. Christou, Polyhedron 25 (2006) 613.
[69] C.J. Milios, P.A. Wood, S. Parsons, D. Foguet-Albiol, C. Lampropoulos, G. Christou, S.P. Perlepes, E.K. Brechin, Inorg. Chim. Acta 360 (2007) 3932.
[70] A.M. Ako, V. Mereacre, R. Clerac, I.J. Hewitt, Y.H. Lan, C.E. Anson, A.K. Powell, Dalton Trans. (2007) 5245.
[71] V.M. Mereacre, A.M. Ako, R. Clerac, W. Wernsdorfer, G. Filoti, J. Bartolomé, C.E. Anson, A.K. Powell, J. Am. Chem. Soc. 129 (2007) 9248.
[72] A.M. Ako, V. Mereacre, R. Clérac, I.J. Hewitt, Y. Lan, G. Buth, C.E. Anson, A.K. Powell, Inorg. Chem., submitted for publication.
[73] M.A. Aldamen, J.M. Clemente-Juan, E. Coronado, C. Marti-Gastaldo, A. Gaita-Arino, J. Am. Chem. Soc. 130 (2008) 8874.
[74] M.T. Gamer, Y. Lan, P.W. Roesky, A.K. Powell, R. Clerac, Inorg. Chem. 47 (2008) 6581.
[75] R. Bircher, B.F. Abrahams, H.U. Guel, C. Boskovic, Polyhedron 26 (2007) 3023.
[76] L.G. Westin, M. Kritikos, A. Caneschi, Chem. Commun. 1012 (2003).
[77] K.L. Taft, C.D. Delfs, G.C. Papaefthymiou, S. Foner, D. Gatteschi, S.J. Lippard, J. Am. Chem. Soc. 116 (1994) 823.
[78] T. Kajiwara, K. Katagiri, S. Takaishi, M. Yamashita, N. Iki, Chem. Asian J. 1 (2006) 349.
[79] J.K. Tang, I. Hewitt, N.T. Madhu, G. Chastanet, W. Wernsdorfer, C.E. Anson, C. Benelli, R. Sessoli, A.K. Powell, Angew. Chem. Int. Ed. 45 (2006) 1729.
[80] J.P. Costes, F. Dahan, F. Nicodeme, Inorg. Chem. 40 (2001) 5285.
[81] J. Luzon, K. Bernot, I.J. Hewitt, C.E. Anson, A.K. Powell, R. Sessoli, Phys. Rev. Lett. 100 (2008) (art. no. 247205).
[82] L.F. Chibotaru, L. Ungur, A. Soncini, Angew. Chem. Int. Ed. 47 (2008) 4126.
[83] K. Bernot, L. Bogani, A. Caneschi, J. Luzon, M. Etienne, C. Sangregorio, M. Shanmugam, R. Sessoli, D. Gatteschi, submitted for publication.
[84] K. Bernot, J. Luzon, L. Bogani, A. Caneschi, D. Gatteschi, R. Sessoli, A. Vindigni, A. Rettori, M.G. Pini, submitted for publication.
[85] N. Ishikawa, M. Sugita, W. Wernsdorfer, J. Am. Chem. Soc. 127 (2005) 3650.
[86] N. Ishikawa, M. Sugita, W. Wernsdorfer, Angew. Chem. Int. Ed. 44 (2005) 2931.
[87] M. Trif, F. Troiani, D. Stepanenko, D. Loss, Phys. Rev. Lett. 101 (2008) (art. no. 217201).